PCCP

Accepted Manuscript

ROYAL SOCIETY OF CHEMISTRY

www.rsc.org/pccp

Effect of *in situ* synthesized Fe_2O_3 and Co_3O_4 nanoparticles on electroactive β phase crystallization and dielectric properties of poly(vinylidene fluoride) thin films

Pradip Thakur[1], Arpan Kool[1], Biswajoy Bagchi[2], Sukhen Das[1]*, Papiya Nandy[1]

[1]Department of Physics, Jadavpur University, Kolkata- 700032, India
[2]Fuel Cell and Battery Division, Central Glass and Ceramic Research Institute, Kolkata-700032, India.
*Corresponding author. Email address: sdasphysics@gmail.com, Mobile: +919433091337

ABSTRACT:

A simple and low cost *in situ* process have been developed to synthesize Fe_2O_3/Co_3O_4 nanoparticles (NPs) loaded poly(vinylidene fluoride) (PVDF) thin films. The electroactive β phase nucleation mechanism and the dielectric properties of the films have been investigated by X-ray diffraction spectra, Fourier transform infrared spectroscopy, differential scanning calorimetry and L.C.R. meter. Results confirmed that the electroactive β phase crystallization in PVDF matrix is due to fast nucleating or catalytic effect of the *in situ* NPs. Homogenous dispersion of *in situ* Fe_2O_3/Co_3O_4 NPs in polymer matrix leads to strong interfacial interaction between the NPs and the polymer resulting in enhanced β phase nucleation in PVDF and large dielectric constant of the thin films. The observed variation in the electroactive β phase nucleation by NPs (Fe_2O_3/Co_3O_4) and the dielectric properties of the thin films have been explained on basis of surface charge, size, geometrical shape and extent of agglomeration of the NPs in polymer matrix.

Keywords: *In situ*, β phase, interfacial polarization, dielectric constant

1. Introduction

Recently, Poly(vinylidene fluoride) (PVDF) and its copolymers such as poly(vinylidene fluoride-trifluoroethylene) [P(VDF-TrFE)], poly(vinylidene fluoride-hexafluoropropylene [P(VDF-HFP)] and poly(vinylidene fluoride-trifluoroethylene-chlorofluoroethylene) [P(VDF-TrFECFE)] based nanocomposites with high dielectric constants are emerging as potential materials for a broad range of applications such as in grid levelling, rail runs, pulsed lasers, electric or hybrid vehicles, communications devices, actuators, artificial muscles, charge-storage capacitors systems etc.[1-8]

PVDF ($[-CH_2-CF_2-]_n$) is a semicrystalline polymer and has mainly five crystalline phases α, β, γ, δ and ε. Among these, α, β and γ phases are most common but melt processing commonly results in dominant non-polar α-phase. Whereas, polar or electroactive β and γ forms, especially β phase, exhibits good piezoelectric, pyroelectric and ferroelectric properties. The α phase has $TGTG^{'}$ (T- trans, G-gauche^{+}, $G^{'}$-gauche) dihedral conformation, β phase has all trans (TTTT) conformation and γ phase has TTTGTTG' conformation.[3, 9]

Accordingly, a lot of research effort has been invested for enhancing electroactive β-phase content in PVDF matrix as well as its dielectric properties introducing nanomodifiers such as clays,[9-12] ceramic fillers,[13, 14] carbon black, [15, 16] carbon nanotubes,[17, 18] carbon nanofibers,[19-21] graphene,[22] quaternary phosphorus salt functionalized graphene,[23] metal nanoparticles

(NPs),[24-27] ferrites,[28,29] inorganic salts[30] etc. There are few reports on the addition of metal oxides to improve dielectric properties of PVDF. Increase in dielectric constant by introducing ZnO was reported by both Wu et al.,[31] and Zhang et al.[32] Rozana et al., reported dielectric constant value 21 with the addition of 7% MgO NPs in PVDF.[33] Bhatt et al., reported about the crystallinity, magnetic and electrochemical properties of PVDF/ Co_3O_4 composites but no attention has been paid about β phase nucleation and dielectric properties.[34]

Most recently, *in situ* synthesis of metal or metal oxide NPs in PVDF matrix have gained tremendous interest of the researches because of the well homogenous dispersion of the NPs in the polymer matrix granted good interactions between the NPs and polymer, than the traditional solution phase mechanical mixing of the NPs and the polymer. There are however few reports of *in situ* synthesis of different metal or metal oxides NPs in PVDF matrix with the intention to enhance electroactive β phase crystallization and dielectric properties. Enhancement of electroactive β phase orientation in PVDF by *in situ* synthesized ZnO nanowires,[35] Au[26] and Pd[27] NPs have been reported. Deepa et al., showed a low percolation threshold of 7 volume% for *in situ* synthesized Ag NPs in PVDF than the ultrasonic mixing composites of Ag powder and PVDF. The homogenous dispersion of *in situ* Ag NPs in PVDF leads to percolation at lower filler loading.[25]

The present study involves incorporation of Fe_2O_4 and Co_3O_4 NPs in PVDF matrix by *in situ* process and their significant effect on the nucleation of electroactive β phase, crystallinity and dielectric properties of the polymer films..

2. Results and Discussion

2.1. X-ray diffraction analysis

The crystallization behaviour of the films and the formation of Fe_2O_3 or Co_3O_4 NPs were investigated by the X-ray diffractometer. Figure 1a and b shows the X-ray diffraction (XRD) patterns of the Fe_2O_3 and Co_3O_4 NPs modified PVDF films respectively.

In Figure 1a the XRD peaks around $2\theta = 32^o$, 45.3^o and 56.2^o correspond to (222), (332) and (440) planes confirmed the formation of nano-sized Fe_2O_3 (JCPDS No. 32-0469 and 39-0238) and the peaks around $2\theta = 32.1^o$, 36.9^o, 39.5^o, 45.8^o, 50.1^o and 56.6^o correspond to (220), (311), (222), (400), (331) and (422) planes in Figure 1b confirmed the formation of Co_3O_4 NPs (JCPDS No. 43-1003) in the polymer nanocomposite films.

The diffraction pattern of pure PVDF shows peaks at 2θ values of 17.6^o (100), 18.2^o (020), 19.9^o (021) and 26.4^o ((201), (310)) corresponding to α phase and 38.9^o (211) for γ phase. But for the nanocomposite films all peaks corresponding to α or γ phases were disappeared only one characteristic peak of PVDF at 20.5^o ((110), (200)) for Fe_2O_3 NPs loaded samples and at 20.7^o ((110), (200)) for Co_3O_4 NPs loaded samples appeared which confirmed the nucleation of electroactive β phase in nanocomposite films.[9, 36] Thus the nucleation of electroactive β phase is significantly accelerated with increasing content for both the NPs. Closer observation of both the X-ray diffractograms showed that the intensity of main β phase peak

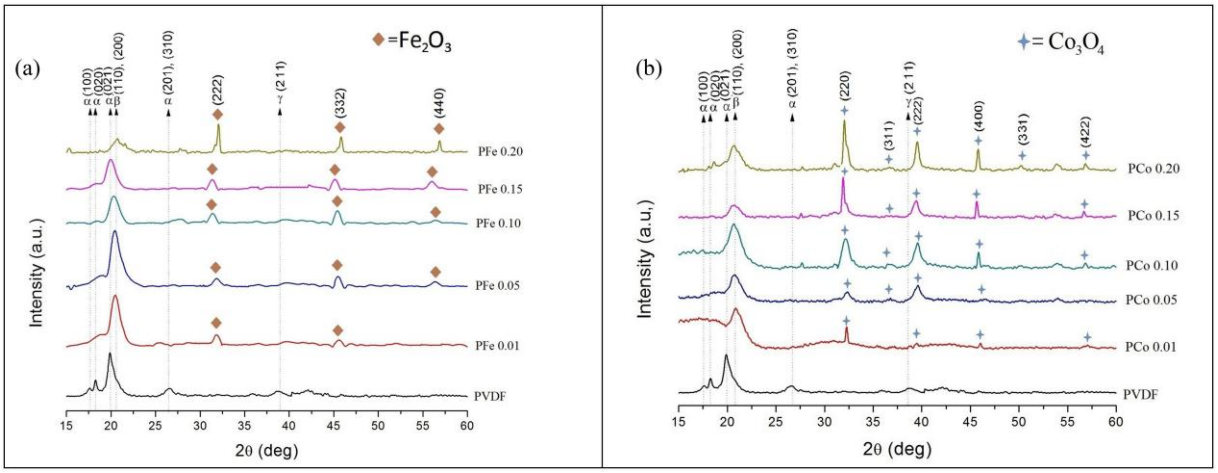

Figure 1: XRD of pure PVDF and the NPs loaded thin films; (a) Fe_2O_3 NPs loaded PVDF films and (b) Co_3O_4 NPs loaded PVDF thin films.

((110), (200)) was increased upto 2.6 volume% doping of Fe_2O_3 NPs and 6.6 volume% doping of Co_3O_4 NPs. Thus the nucleation of electroactive β phase is relatively more accelerated at a low concentration of Fe_2O_3 NPs than Co_3O_4 NPs. This dissimilarity in nucleating action may be due to the morphological, structural and surface charge differences between the NPs.

2.2. Fourier transform infrared spectroscopy

Figure 2a and 3a show the Fourier transform infrared (FTIR) spectra of pure PVDF and the Fe_2O_3/Co_3O_4 NPs doped PVDF films. FTIR spectrum of the films provides the valuable information about their structure distinguishing the different crystalline polymorphs of the PVDF. The spectrum of pure PVDF shows characteristic absorbance bands at 489 cm^{-1} (CF_2 waging) 533 cm^{-1} (CF_2 bending), 615 and 764 cm^{-1} (CF_2 bending and skeletal bending), 795 and 975 cm^{-1} (CH_2 rocking) correspond to α-phase and tiny absorbance band at 840 cm^{-1} (CH_2 rocking, CF_2 stretching and skeletal C-C stretching) is due to β phase. However, for both NPs doped PVDF films all characteristic absorbance bands due to α phase are completely disappeared and only characteristic absorbance bands due to electroactive β phase at 475 cm^{-1} (CF_2 deformation) 510 cm^{-1} (CF_2 stretching), 600 cm^{-1} (CF_2 wag) and 840 cm^{-1} (CH_2 rocking, CF_2 stretching and skeletal C-C stretching) have been appeared strongly. [9, 36, 37] In the case of Fe_2O_3 NPs doped PVDF the intensity of β-PVDF characteristic bands are significantly improved upto 2.6 volume% doping and then decrease for higher NPs content. And for Co_3O_4 NPs doped PVDF the improvement of intensities of β-PVDF characteristic bands are observed upto 6.6 volume% doping of the NPs.

The relative fraction of electroactive β phase content ($F(\beta)$) in the NPs doped PVDF films have been calculated using equation 1 and variation of $F(\beta)$ (%) with Fe_2O_3/Co_3O_4 NPs content (volume%) have been shown graphically in Figure 2b and 3b. The β phase content increases with NPs concentration for all the cases. An interesting fact is that only 2.6 volume% Fe_2O_4 NPs is needed to achieve $F(\beta)$ values 71% (Figure 2b) whereas 6.6 volume%

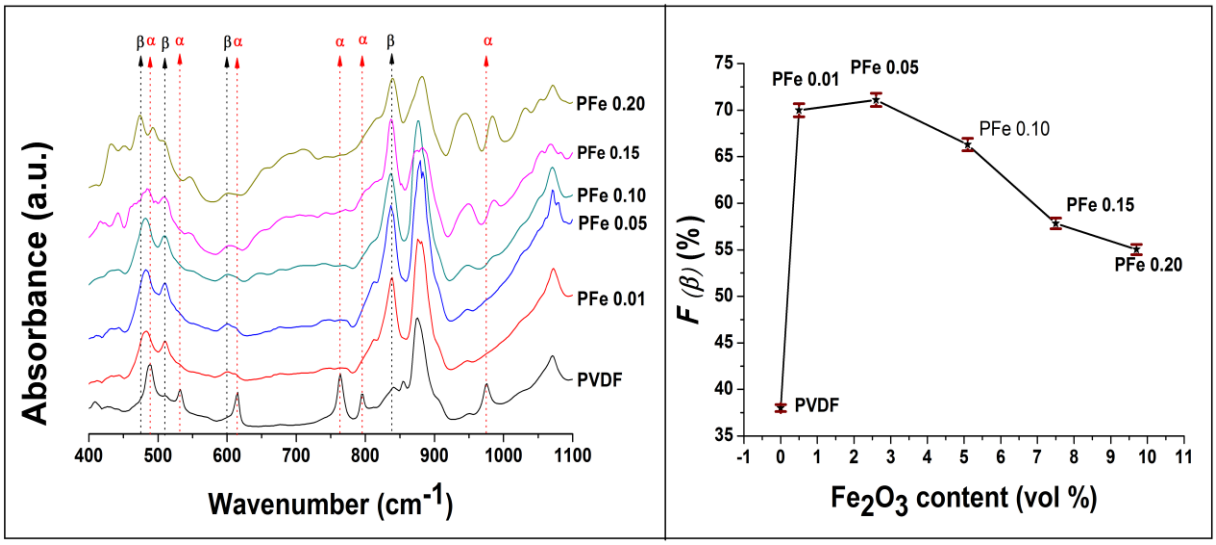

Figure 2: (a) FTIR spectra of pure PVDF and Fe_2O_3 NPs loaded PVDF thin films (PFe 0.01, PFe 0.05, PFe 0.10, PFe 0.15 and PFe 0.20) and (b) Evaluation of β-phase content with increasing Fe_2O_3 NPs content form IR spectra. Error bars represent the standard deviation of the experiment conducted in triplicate and were assessed by one way ANOVA using graph pad Instat version 5.0 software.

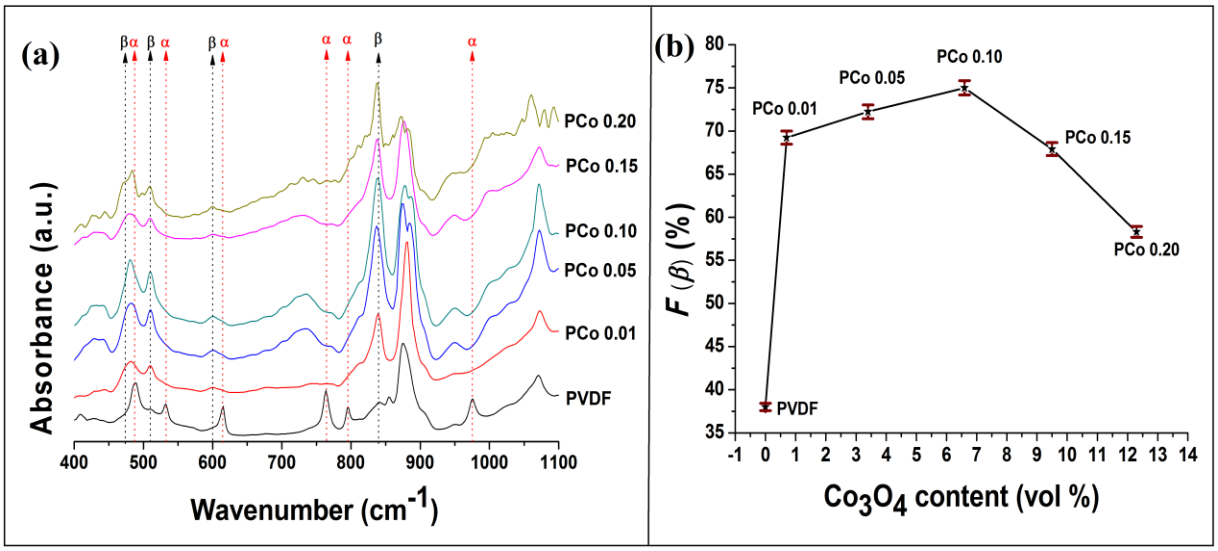

Figure 3: (a) FTIR spectra of pure PVDF and Co_3O_4 NPs loaded PVDF thin films (PCo 0.01, PCo 0.05, PCo 0.10, PCo 0.15 and PCo 0.20) and (b) Evaluation of β-phase content with increasing Co_3O_4 NPs content form IR spectra. Error bars represent the standard deviation of the experiment conducted in triplicate and were assessed by one way ANOVA using graph pad Instat version 5.0 software.

Co_3O_4 NPs is needed for achieving 75% (Figure 3b) β phase content in PVDF. Thus, it is also evident from FTIR spectroscopy that the β phase stabilization and nucleation is more accelerated by Fe_2O_4 NPs than Co_3O_4 NPs.

2.3. Differential scanning calorimetry

Differential scanning calorimetry (DSC) has been used for the identification of the crystalline phase of PVDF as a complementary techniques of XRD and FTIR. Figure 4 shows the DSC

thermographs of pure PVDF and the NPs loaded PVDF samples. The DSC thermograph of pure PVDF shows a strong melting peak at 163.62 ^{o}C suggested for α phase crystallization

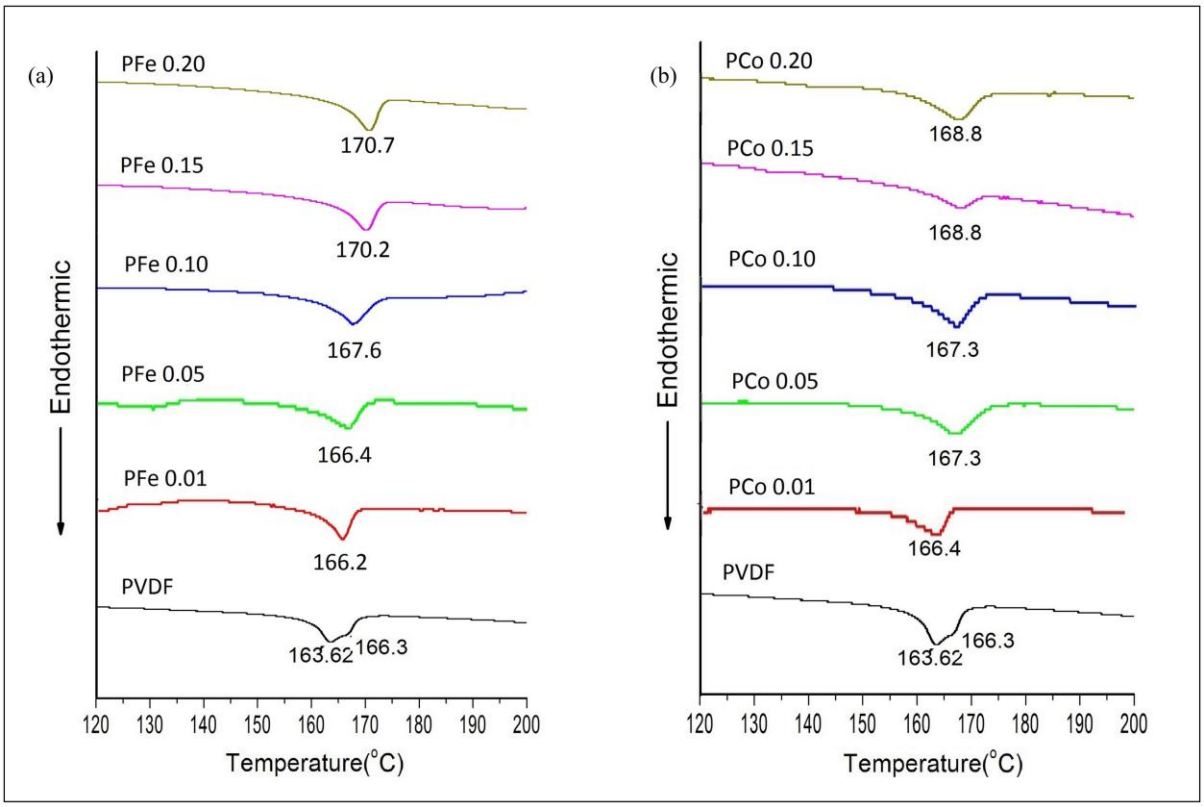

Figure 4: (a) DSC thermographs of pure PVDF and Fe_2O_3 NPs loaded PVDF thin films (PFe 0.01, PFe 0.05, PFe 0.10, PFe 0.15 and PFe 0.20) and (b) DSC thermographs of pure PVDF and Co_3O_4 NPs loaded PVDF thin films (PCo 0.01, PCo 0.05, PCo 0.10, PCo 0.15 and PCo 0.20).

and a very small peak at 166.3 ^{o}C suggested for some presence of electroactive β phase content in pure PVDF that also observed in FTIR. But for all NPs loaded PVDF films the melting temperatures (T_m) shifted to higher temperatures by 3 to 7 ^{o}C for Fe_2O_4 NPs loaded samples and by 3 to 5 ^{o}C for Co_3O_4 NPs loaded samples with increasing loading concentrations. So, this DSC results suggest to more electroactive β phase crystallization in both NPs doped PVDF films which are consistent with the XRD and FTIR data. [9, 12, 18, 36]

DSC thermographs also give the information about the degree of crystallinity of the films. First, the melting enthalpies (ΔH_m) of pure PVDF and the NPs loaded PVDF films are determined from the DSC thermographs and then the degree of crystallinity (X_c) of the samples have been calculated using equation 2. Figure 5 shows the variation of ΔH_m and X_c with the doping concentration of the NPs. Increase in melting enthalpies, ΔH_m have been observed due to NPs (Fe_2O_3 and Co_3O_4) loading in PVDF (Figure 5a and c) implying an increase in the degree of crystallinity of PVDF.

Figure 5b and d show the changes of X_c of the samples with Fe_2O_3 and Co_3O_4 NPs loading concentrations. The X_c values increase with the NPs content and achieve maximum about 55.7% for 2.6 volume% doping of Fe_2O_4 NPs (PFe 0.05) where about 56.7% for 6.6

volume% of Co_3O_4 NPs (PCo 0.10). Further doping of the Fe_2O_4 or Co_3O_4 NPs gradually decreased the X_c. For lower doping upto 2.6 volume% for Fe_2O_3 NPs and 6.6 volume % for

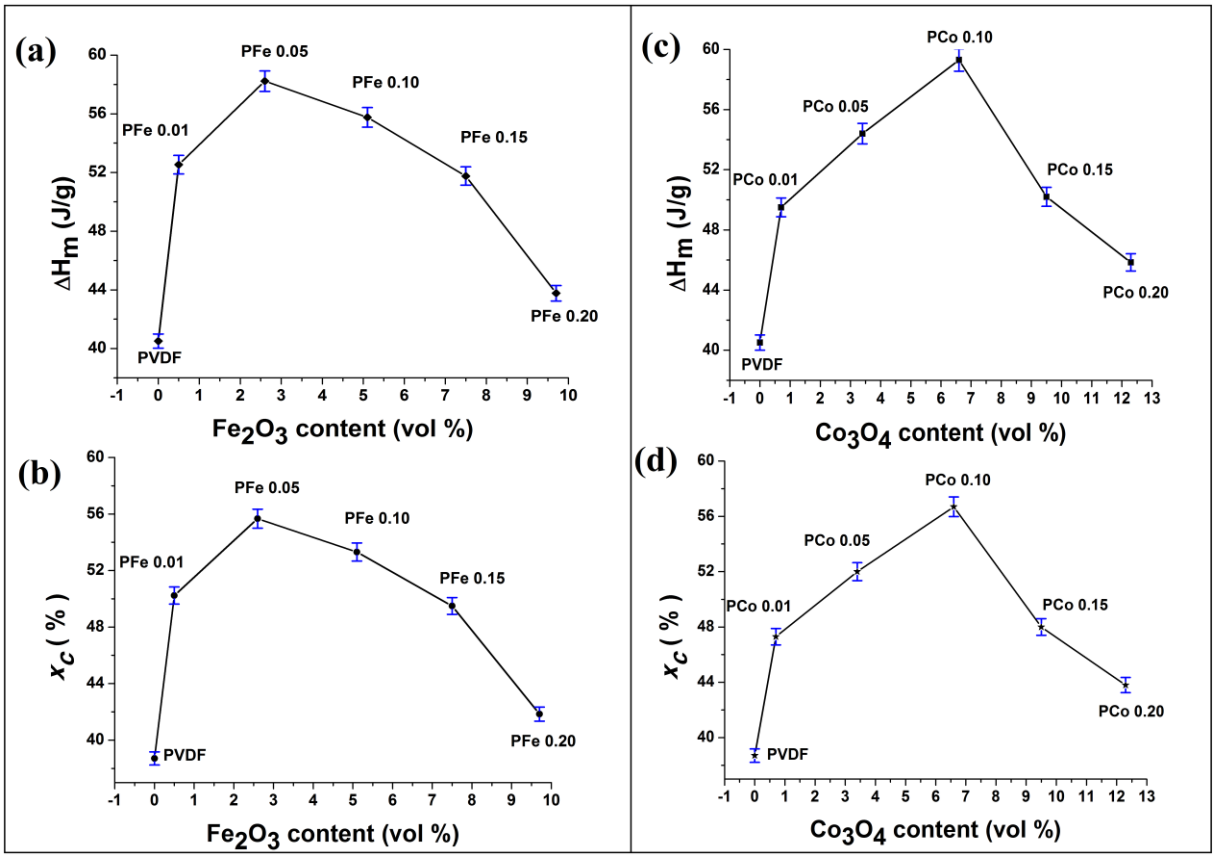

Figure 5: Evaluation of enthalpy of fusion (a, c) and degree of crystallinity (b, d) of pure PVDF and Fe_2O_3/ Co_3O_4 NPs loaded PVDF thin films with increasing NPs content from DSC thermographs. Error bars represent the standard deviation of the experiment conducted in triplicate and were assessed by one way ANOVA using graph pad Instat version 5.0 software.

Co_3O_4 NPs the increase in crystallinity may be due to the nucleating action of the NPs. Higher doping of the NPs in PVDF may lead to confinement of movement of polymer chains[9] and formation of electroactive β phase grains as the number of nucleation points grows so much that the spherulites i.e. grains cannot be formed. [18, 38] This is why, the X_c is decreased.

2.4. Field emission scanning electron microscopy (FESEM)

Figure 6 and 7 show the morphology and microstructures of pure and Fe_2O_3/Co_3O_4 NPs doped PVDF films as well as the formation of NPs in PVDF matrix. In Fe_2O_3 NPs loaded samples well distribution of the *in situ* NPs has been observed upto 5.1 volume% doped films and for higher salt concentration the NPs have been agglomerated in the PVDF matrix. For PFe 0.01 and PFe 0.05 samples formation of brick like Fe_2O_4 NPs are observed (Figure 6).

The images of Co_3O_4 loaded films (Figure 7) confirm the formation of Co_3O_4 NPs of average particle size 30-80 nm. Fine and homogenous distribution and no such agglomeration of the

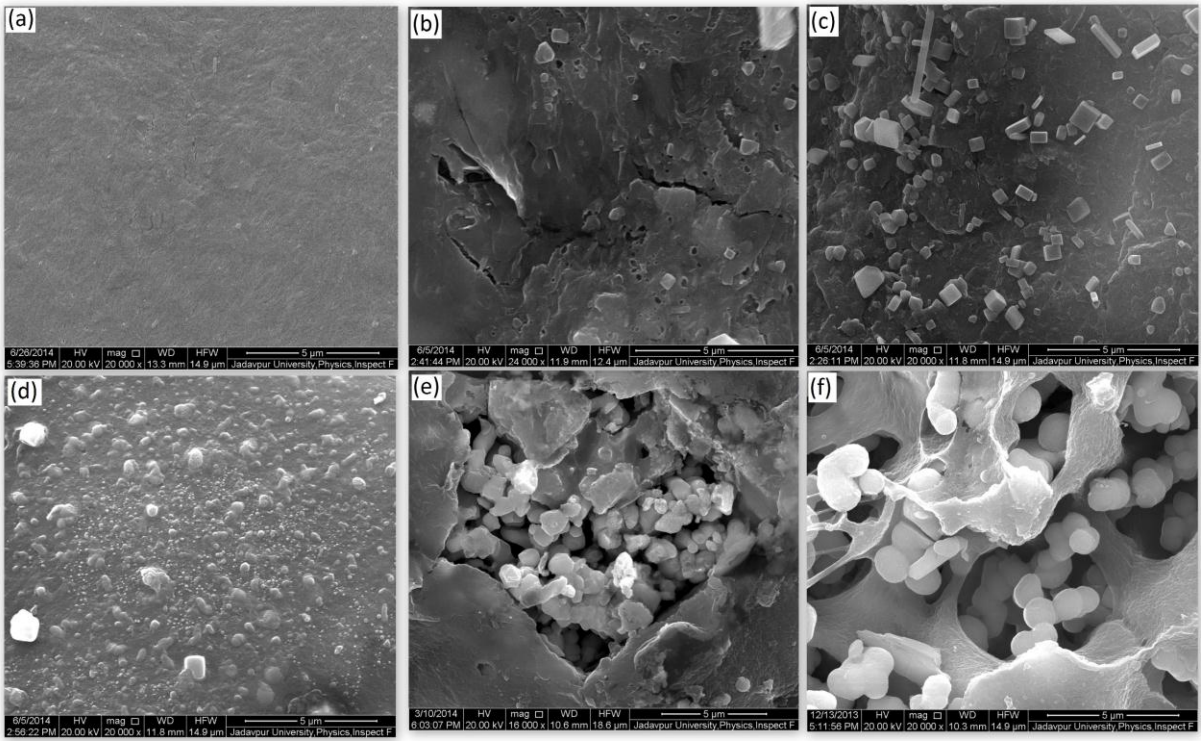

Figure 6: FESEM images of pure PVDF and the Fe_2O_3 NPs loaded PVDF thin films films (PFe 0.01, PFe 0.05, PFe 0.10, PFe 0.15 and PFe 0.20).

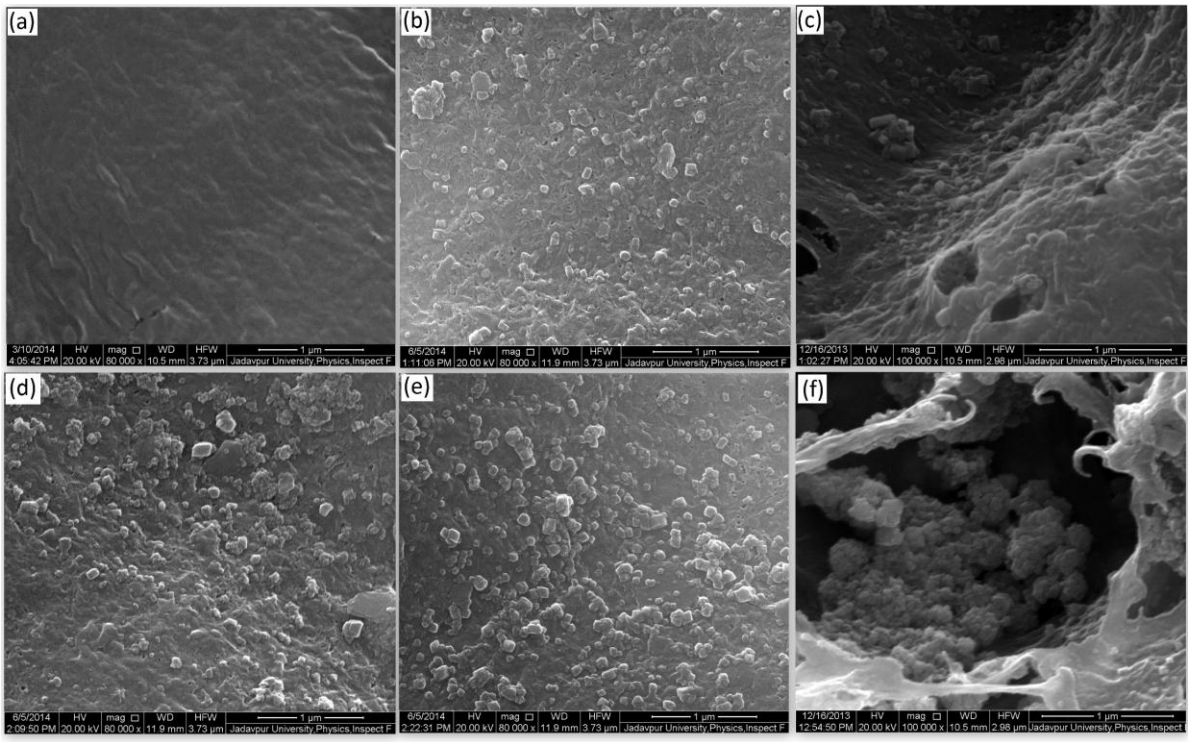

Figure 7: FESEM images of pure PVDF and and Co_3O_4 NPs loaded PVDF thin films (PCo 0.01, PCo 0.05, PCo 0.10, PCo 0.15 and PCo 0.20).

in situ NPs have been found upto 9.5 volume% doping in PVDF. For further increase in the salt concentration agglomeration of the *in situ* NPs in polymer matrix is observed.

2.5. Electroactive β-phase formation mechanism in PVDF

Though the interface of Fe_2O_3 or Co_3O_4 NPs/PVDF is proven in FESEM images (Figure 6 and 7) and the formation of electroactive β phase has been confirmed by XRD, FTIR and DSC data (Figure 1 to 5), it is necessary to analysis the origin of this interaction between the NPs and the polymer which promotes the electroactive β phase nucleation. Our previous study on clay-PVDF nanocomposites propose the strong interaction between the positive CH_2 dipoles of PVDF and the negatively charged surfaces of the clay minerals lead to the alignment of stabilized chains in longer all trans conformation on the clay mineral surfaces.[9] Thus, to explain the origin of β phase crystallization in our present work, the surface charges of the *in situ* NPs have been investigated.

The possible electrostatic charge on the surface of the Fe_2O_3 or Co_3O_4 NPs synthesized in DMSO medium without adding PVDF discussed in experimental section 2.3 has been investigated by zeta potential analysis. The zeta potential has been studied at the same pH of corresponding NPs-PVDF mixture in DMSO (pH= 5.7 for Fe_2O_3 NPs ant pH= 5.9 for Co_3O_4 NPs). The obtain results of zeta potential distribution have been shown in Figure 8. Both NPs show negative zeta potentials but Fe_2O_3 NPs shows quit higher zeta potential than Co_3O_4 NPs.

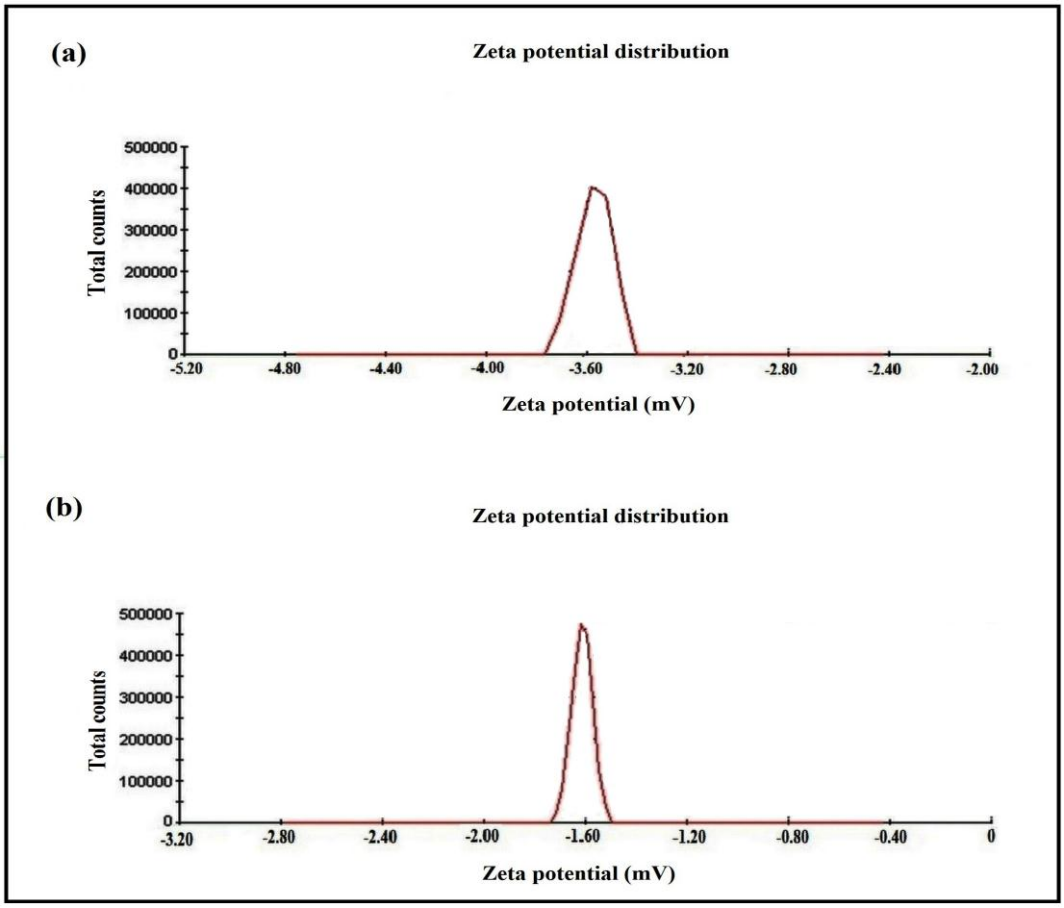

Figure 8: Zeta potential distribution of (a) Fe_2O_3 NPs and (b) Co_3O_4 NPs.

Thus, the nucleation of electroactive β phase takes place on the negatively charged surfaces of Fe_2O_3 or Co_3O_4 NPs. The positive CH_2 dipoles of PVDF chains suffers strong electrostatic interaction with negatively charged surface of the NPs resulting in stabilized longer TTTT or all trans conformation on the NPs surfaces.[9, 28] Figure 9 shows the ion-dipole or electrostatic interaction mechanism between the NPs and polymer chains during the formation of electroactive β-phase. The activity to enhance the β phase nucleation in PVDF of Fe_2O_3 NPs is more than Co_3O_4 NPs which also confirmed by XRD and FTIR.

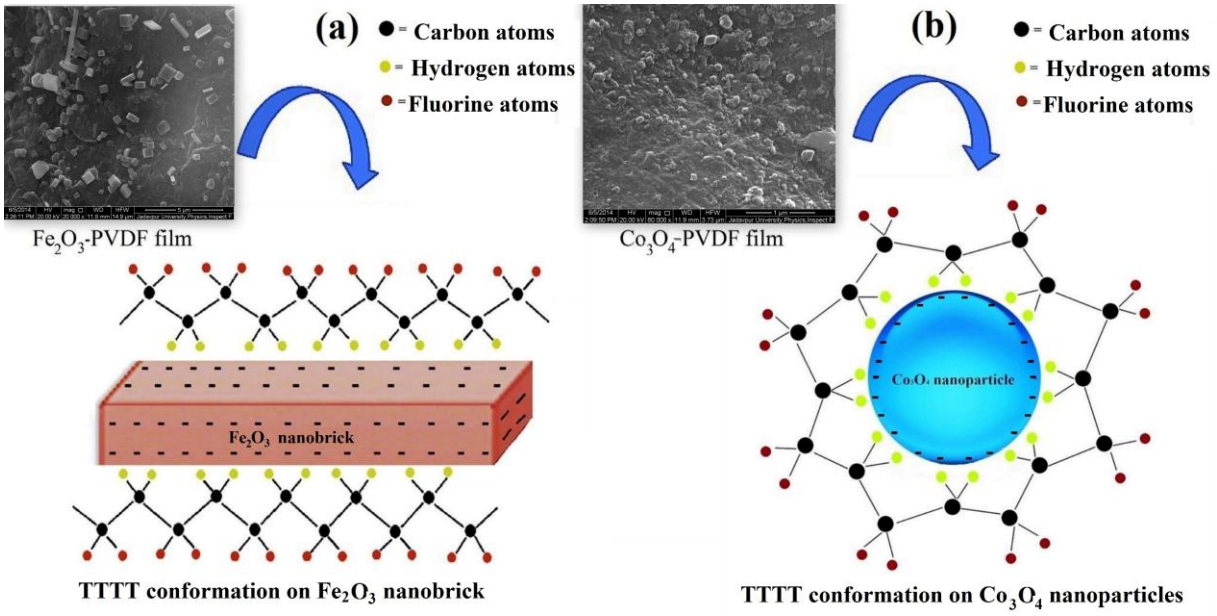

Figure 9: Schematic diagram of proposed β phase transformation mechanism.

About 71 % β phase crystallization has been reached in PVDF by 2.6 volume% content for Fe_2O_3 NPs where 6.6 volume% Co_3O_4 NPs is needed to reach about 75% β phase content (Figure 2 and 3). This difference in activity to promote β phase nucleation in PVDF is due to the difference in zeta potential, size and surface morphology of the NPs (Figure 6 to 8). Since the surface of the Fe_2O_3 NPs is more negatively charged than Co_3O_4 NPs, the electrostatic or ion-dipole interaction is stronger in Fe_2O_3 NPs loaded PVDF samples. So, the more negatively charged large flat surfaces of the brick like Fe_2O_3 NPs are more suitable for the alignment of the stabilized polymer chains in longer TTTT conformation than the less negatively curved surfaces of Co_3O_4 NPs.[9, 28] A similar observation was also reported in our previous study, where negatively charged large flat surfaces of kaolinite plates are seems to be more suitable for the alignment of stabilized in all trans conformation on kaolinite plates than the negatively charged curved surfaces of halloysite nanotubes.[9]

2.6. Dielectric properties

2.6.1. Dependence of dielectric properties on NPs content

Figure 10 shows the variation of dielectric constant and tangent loss of the Fe_2O_3 /Co_3O_4 NPs loaded PVDF films as a function of NPs content at 100 Hz. The dielectric constant increases almost sharply in a linear fashion for Fe_2O_3 NPs loaded polymer films upto 5.1 volume% doping of Fe_2O_3 NPs and decreases for higher doping content (Figure 10a). For Co_3O_4 NPs

loaded samples linearly increase in dielectric constant has been observed upto 6.6 volume% loading but a giant dielectric constant is observed for 9.5 volume% loading which may be due to reaching the percolation threshold. Further doping of Co_3O_4 NPs decreases the value of dielectric constant (Figure 10b). Maximum dielectric constant is found 1027 for PFe 0.10 sample (5.1 volume% doping of Fe_2O_3 NPs) and 5963.6 for PCo 0.15 sample (9.5 volume% doping of Co_3O_4 NPs). Tangent losses of Fe_2O_3 NPs loaded films increase almost linearly with Fe_2O_3 NPs content (Figure 10a). But a nonlinear increase in tangent loss like dielectric constant is observed for Co_3O_4 NPs loaded samples.

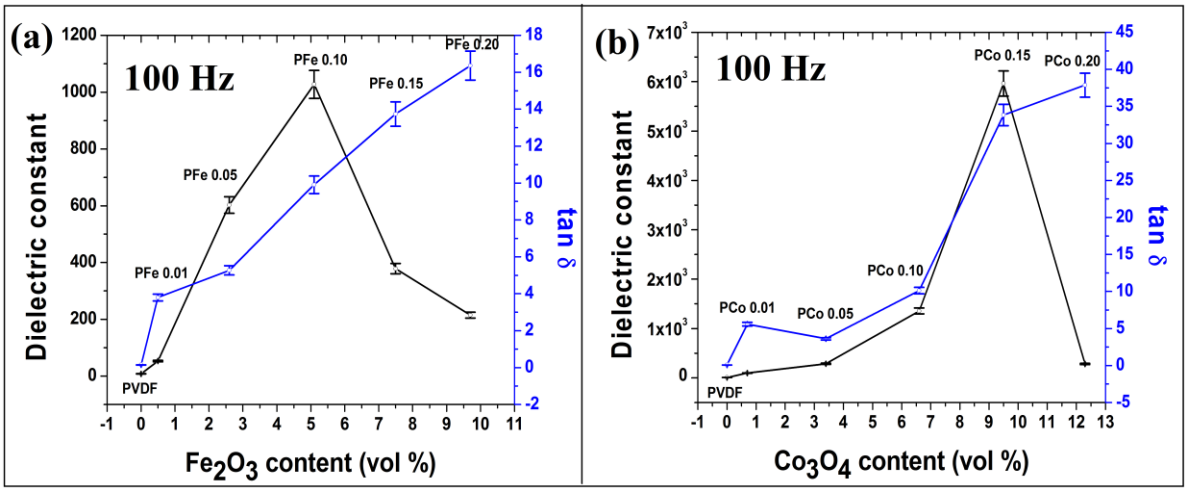

Figure 10: NPs content dependence of dielectric constants and tangent losses at 100 Hz; (a) the Fe_2O_3 NPs loaded PVDF thin films (PFe 0.01, PFe 0.05, PFe 0.10, PFe 0.15 and PFe 0.20) and (b) Co_3O_4 NPs loaded PVDF thin films (PCo 0.01, PCo 0.05, PCo 0.10, PCo 0.15 and PCo 0.20). Error bars represent the standard deviation of the experiment conducted in triplicate and were assessed by one way ANOVA using graph pad Instat version 5.0 software.

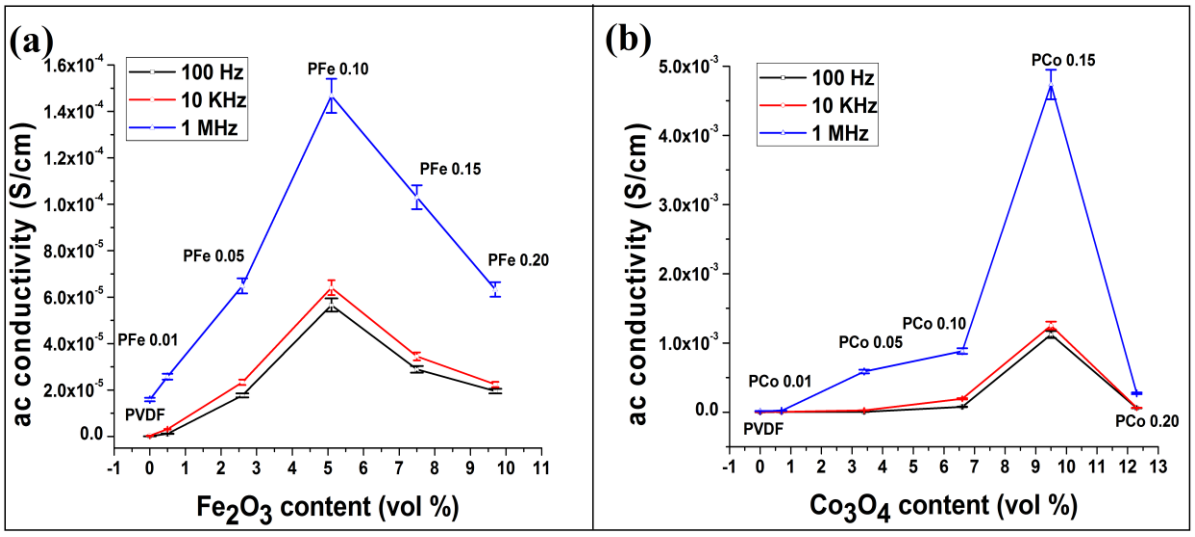

Figure 11: NPs content dependence of ac conductivities at 100 Hz, 10 KHz and 1 MHz; (a) the Fe_2O_3 NPs loaded PVDF thin films (PFe 0.01, PFe 0.05, PFe 0.10, PFe 0.15 and PFe 0.20) and (b) Co_3O_4 NPs loaded PVDF thin films (PCo 0.01, PCo 0.05, PCo 0.10, PCo 0.15 and PCo 0.20). Error bars represent the standard deviation of the experiment conducted in triplicate and were assessed by one way ANOVA using graph pad Instat version 5.0 software.

Figure 11a and b show the dependence of ac conductivities of the samples on Fe_2O_3 and Co_3O_4 NPs loading concentrations respectively at 100 Hz, 10 KHz and 1 MHz. Sharp increase in ac conductivity with Fe_2O_3 NPs content has been observed upto 5.1 volume% in all three frequencies and then decreases for higher doping of NPs in PVDF (Figure 11a). And like dielectric constant, a sharp increase in ac conductivity at 9.5 volume% loading Co_3O_4 NPs is also observed for Co_3O_4 NPs loaded PVDF films.

The enhancement of dielectric properties can be explained by two main factors. First one is Maxwell-Wagner-Sillars (MWS) interfacial polarization effect which appears in heterogeneous medium consisting of phases with different permittivity and conductivity due to accumulation of the charges at the interfaces.[9, 39-43] At low NPs concentration, the NPs are well separated from each other with no such effective interaction between them. With increase in NPs content, number of NPs and their interfacial area per unit volume increases while the interparticle distance decreases. This improves the average polarization associated with the NPs and the coupling between neighboring grains, resulting to the giant dielectric enhancement of the percolative nanocomposite films. The observed dielectric nature of the samples also may be explained from their microstructures (FESEM). Well homogeneous dispersion of the NPs in PVDF matrix upto 5.1 volume% loading of Fe_2O_3 NPs and 9.5 volume% loading of Co_3O_4 NPs result more interfacial area per unit volume of the NPs which improves the interfacial polarization in the samples. Higher doping concentrations of the NPs decrease the interfacial area per unit volume due to agglomeration of the NPs, (Figure 6 and 7) resulting decrease in dielectric constant and ac conductivity.[25] And the second factor is the electroactive β phase content present in the polymer nanocomposite samples. The improvement of polarization in the NPs loaded samples is also attributed to the improved interface between NPs and electroactive phases of PVDF. Figure 9 illustrates the interaction between the NPs and polymer matrix. Strong dipolar interaction between the negatively charged NPs surfaces and the $-CH_2$ dipoles of PVDF contributed partially to the colossal dielectric properties of Fe_2O_4/Co_3O_4 NPs loaded PVDF thin films.

The dissimilarity between the threshold values of the two NPs loaded PVDF films (about 5.1 volume% for Fe_2O_3 NPs and 9.5 volume% for Co_3O_4 NPs) also observed. This fact is also readily explained by the geometrical shape of the two NPs (Figure 6 and 7). The Fe_2O_3 NPs are brick like whose intersection probability is more than the spherical Co_3O_4 NPs. So, Fe_2O_3 NPs facilitate the formation of percolation network in polymer matrix at low concentration than Co_3O_4 NPs loaded polymer samples. More charges on the Fe_2O_3 NPs surfaces affect strongly the electric field distribution than Co_3O_4 NPs (Figure 8). Thus, local field enhancements are more likely to take place in brick like Fe_2O_3 NPs loaded polymer matrix than for spherically shaped Co_3O_4 NPs loaded samples and strengthen the polarization of the neighbouring polymer matrix.[41, 42]

2.6.2. Frequency dependence of the dielectric properties

Figure 12 shows the dependence of the dielectric properties of the Fe_2O_3/ Co_3O_4 NPs loaded PVDF films on the frequency at room temperature and atmospheric pressure.

The dielectric constant of pure PVDF does not vary much with frequency. But its nanocomposite films with different loading of NPs show noticeable steplike decrease in dielectric constant toward high frequency (Figure 12a and d) accompanied by tangent loss peaks at different lower frequencies for different contents of two NPs (Figure 12b and e). Such Debye like dipolar relaxations are mainly for a large dielectric response at lower frequency range (20 Hz to 1 KHz). The steplike decrease in dielectric constant with frequency may be explained by MWS interfacial polarization mechanism.[42, 43]

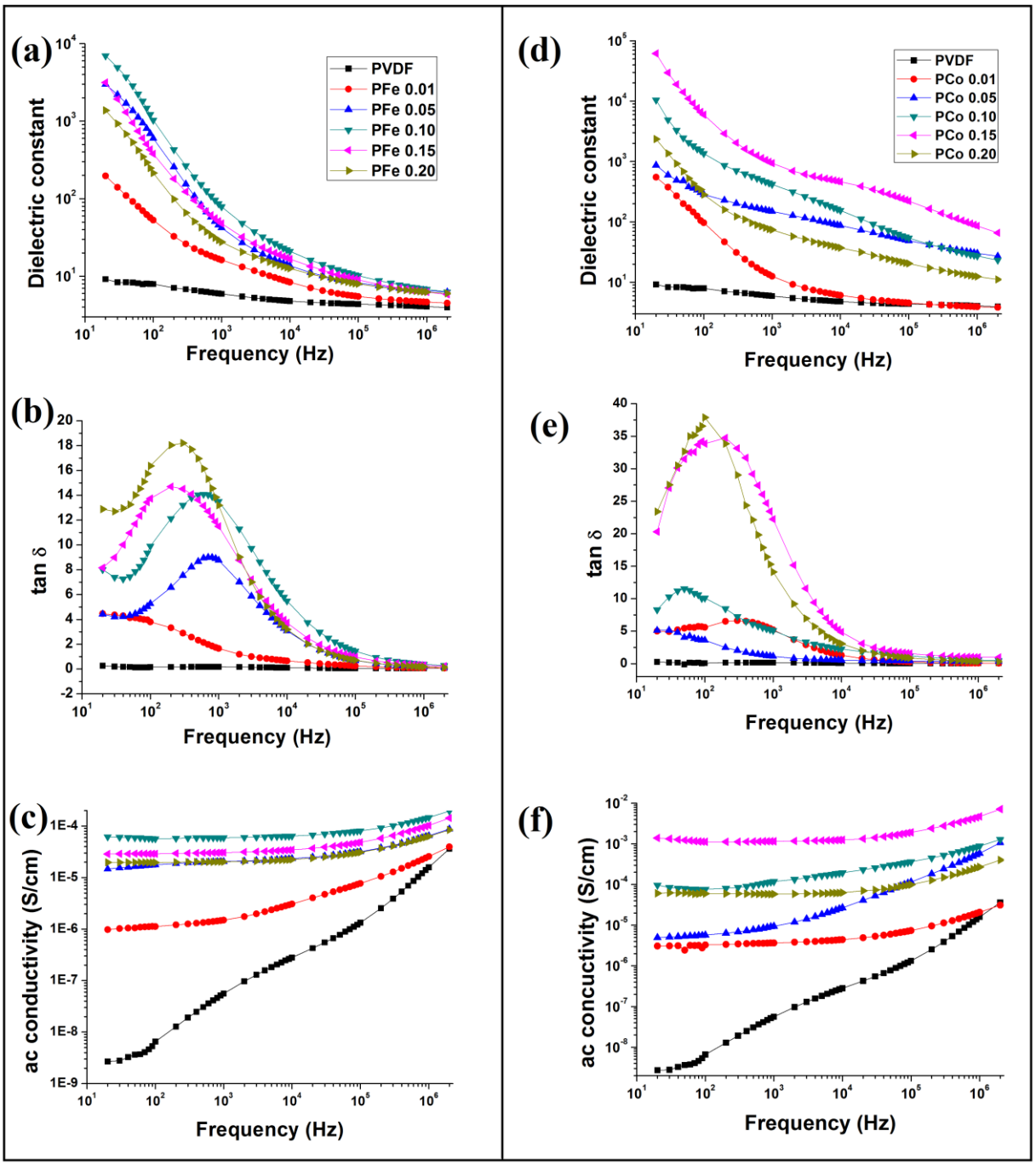

Figure 12: Frequency dependence of dielectric properties of pure PVDF and Fe_2O_3/ Co_3O_4 NPs loaded PVDF thin films; (a, d) dielectric constants, (b,e) tangent losses and (c,f) ac conductivity.

Large interface-to-volume ratios of the NPs intensify their interaction with PVDF matrix. When an electric field is applied on the samples, the space charge accumulation and short-range dipole-dipole interactions at the interfaces of the conducting NPs-insulating PVDF result in large interfacial polarization as well as large dielectric constant at lower frequencies. Interfacial polarization in NPs doped samples decreased with increasing frequency, which may be due the confinement of charge carriers in the samples, so that their movement and accumulation process needs to have a relatively long time.[39] About 6.962 x 10^3 and 6.17 x 10^4 dielectric constants have been found for 5.1 volume% Fe_2O_3 NPs and 9.5 volume% Co_3O_4 NPs doping in PVDF at 20 Hz (Figure 12a and d). Thus, the dielectric constant of 9.5 volume% Co_3O_4 NPs loaded sample (PCo 0.15) is about 10 times greater than the 5.1 volume% Fe_2O_3 NPs loaded sample (PFe 0.10). This is because of the large accumulation of charge carriers at the interfaces of Co_3O_4 NPs/PVDF. Smaller size of Co_3O_4 NPs than the Fe_2O_3 NPs leads to good homogeneous dispersion of Co_3O_4 NPs in the polymer matrix at higher concentration 9.5 volume% (Figure 6 and 7). Thus, higher doping of Co_3O_4 NPs about 1.86 times greater than Fe_2O_3 NPs and large surface area of the small Co_3O_4 NPs lead to large interfacial areas between the NPs and the polymer matrix in PCo 0.15 sample, resulting large accumulation of the charge carriers at the interfaces i.e. large interfacial polarization as well as large dielectric constant than PFe 0.10 sample.[9, 39, 41]

Figure 12c and f show the frequency dependence of ac conductivities of the Fe_2O_3/ Co_3O_4 NPs loaded PVDF films respectively. The conductivity samples may be divided into two different regions. The conductivity at low frequency region is mainly dominated by dc conductivity and at higher frequencies it is characterized by frequency dependent conductivity that evidences the ac conductivity with MWS interfacial polarization effects and dielectric relaxations.[39-43]So, the ac conductivities have been increased with increasing frequencies for all NPs samples. Highest ac conductivity has been observed for PFe 0.10 (6.20 x 10^{-1} S/cm) and PCo 0.15 (1.39 x 10^{-3} S/cm) samples at 20 Hz.

3. Experimental

3.1. Materials

The materials used in the synthesis of nanocomposite thin films are poly(vinylidene fluoride) (Aldrich, Germany. M_w: 275000 (hpc), M_n: 107000), cobalt chloride hexahydrate (Merck, India), iron chloride anhydrous (Merck, India), sodium borohydrate (Merck, India), dimethyl sulfoxide (DMSO) (Merck, India).

3.2. *In situ* synthesis of transition metal oxide NPs in PVDF matrix and hence the nanocomposite films

First, PVDF was dissolved in DMSO (3.33%) at 60 ºC, followed by dissolution of $CoCl_2$, $6H_2O$ or $FeCl_3$ corresponding to different molar concentrations (0.01-0.20 (M)) of the salts in PVDF-DMSO solution. Then, 1 M sodium borohydrate ($NaBH_4$) solution in DMSO slowly added to PVDF-inorganic salts solution under constant magnetic stirring at room temperature and in air. The addition of $NaBH_4$ reduced the transition metals (Fe and Co) to their corresponding oxides NPs (Fe_2O_3/Co_3O_4) in air. Excess $NaBH_4$ has been used to ensure

complete transformation of the metals to their oxides. The nanocomposite films were obtained by casting the Fe_2O_3/Co_3O_4 NPs loaded PVDF solutions in clean Petri dishes and evaporating the solvent in a dust free oven at 80 ^oC for 24 hours. Pure PVDF film was also prepared at same temperature. All samples were then conserved in vacuum for further studies. The average thickness of as prepared films was in the range of 80-100 µm. The different amount of *in situ* synthesized Fe_2O_3 or Co_3O_4 NPs in the polymer matrix from different concentration of the salts (0.01-0.20 (M)) have been tabulated in Table 1.

Table 1 Different amount of *in situ* synthesized Fe_2O_3 or Co_3O_4 NPs in the polymer matrix

Name of the Samples	Amount of PVDF taken in 15 ml DMSO (mg)	Amount of salts added (M)	Corresponding percentage of the NPs (volume%)	Name of the NPs
PFe 0.01	500	0.01	0.5	**Fe_2O_3**
PFe 0.05		0.05	2.6	
PFe 0.01		0.10	5.1	
PFe 0.15		0.15	7.5	
PFe 0.20		0.20	9.7	
PCo 0.01	500	0.01	0.7	**Co_3O_4**
PCo 0.05		0.05	3.4	
PCo 0.10		0.10	6.6	
PCo 0.15		0.15	9.5	
PCo 0.20		0.20	12.3	
PVDF	500	0	0	**None**

3.3. Synthesis of Fe_2O_3 and Co_3O_4 NPs for Zeta potential measurements

Different molar concentrations of $CoCl_2$, $6H_2O$ or $FeCl_3$ salts were dissolved in DMSO. Then appropriate amount of 1 M sodium borohydrate ($NaBH_4$) solution in DMSO slowly added to the salts solution under constant magnetic stirring at room temperature and in air. Colour changes to brown and pale bluish confirmed the formation of Fe_2O_3 and Co_3O_4 NPs respectively. The NPs were dried at 80 ^oC and collected for Zeta potential measurements.

3.4. Characterizations

The formation of NPs and β phase nucleation in the nanocomposite films were characterized using X-ray diffractometer (Model-D8, Bruker AXS Inc., Madison, WI) at atmospheric pressure and room temperature using nickel filtered Cu target K_α radiation with scan speed of 0.5 s/step and under an operating voltage of 40 kV with 2θ varying from 15^o to 60^o.

Then the samples were further characterized using Fourier transform infrared spectroscopy (FTIR-8400S, Shimadzu) in the wavenumber range from 400 cm^{-1} to 1100 cm^{-1} with a resolution of 4 cm^{-1}. 100 scans were performed for each sample. The fraction of β-phase ($F(\beta)$) in the nanocomposite films were calculated from IR spectra using Lambert-Beer law which is,

$$F(\beta) = \frac{A_\beta}{\left(\frac{K_\beta}{K_\alpha}\right)A_\alpha + A_\beta} \qquad (1)$$

where, A_α and A_β are the absorbance at 764 cm^{-1} and 840 cm^{-1}, respectively and K_β (7.7 x 10^4 cm^2 mol^{-1}) and K_α (6.1 x 10^4 cm^2 mol^{-1}) are the absorption coefficients at the respective wave number.[9, 28]

The crystallization and melting behaviour of the pure PVDF and nanocomposite films were studied using a differential scanning calorimeter (DSC-60, Shimadzu (Asia Pacific) Pte. Ltd., Singapore). All the samples were heated from 120°C to 200°C at a heating rate of 5°C/min. The instrument was calibrated with an indium standard and all the studies were performed under N_2 gas atmosphere. The degree of crystallinity (X_c) of the films was calculated from DSC thermographs using the following equation:

$$X_c = \Delta H_m / \Delta H_{100\%} \qquad (2)$$

Where, ΔH_m is the melting enthalpy of the films and $\Delta H_{100\%}$ is the melting enthalpy of 100% crystalline PVDF with value 104.6 J/gm.[9]

The microstructure of the nanocomposite films and dispersion of the NPs and their morphology were observed using Field emission scanning electron microscope (FESEM) ((INSPECT F50, Netherlands).

The surface charge of the NPs was determined using Zeta potential measurements. The measurements were carried out with Zeta-sizer-5000 (Malvern Instruments, UK).

The frequency dependent capacitance and $tan\delta$ of the samples were studied using a digital LCR meter (Agilent, E4980A) in a sample holder with circular Ag electrodes at room temperature and pressure. 1 V signal was applied for frequencies in the range between 20 Hz to 2 MHz. The dielectric constant (ε) and the ac conductivity (σ_{ac}) of the samples were calculated using following equations (3) and (4) respectively,

$$\varepsilon = C.d / \varepsilon_0 A \qquad (3) \qquad \text{and} \qquad \sigma_{ac} = 2\pi f \varepsilon_0 \varepsilon \tan\delta \qquad (4)$$

where, C, d, A and $tan\ \delta$ are the capacitance, thickness, area and tangent loss of the samples respectively and f is the frequency in Hz applied across the films and ε_0 is permittivity of free space with value 8.854 x 10^{-12} $F.m^{-1}$.[9]

4. Conclusions

Electroactive Fe_2O_3/Co_3O_4 NPs loaded PVDF thin films with large dielectric constant have fabricated by simple *in situ* formation of NPs in polymer matrix.

Electroactive β phase formation is observed for both NPs. About 71% β phase crystallization is reached for 2.6 volume% Fe_2O_3 NPs modified PVDF films compared to 6.6 volume% of Co_3O_4 NPs to attain 75% electroactive β phase. So, the ability of electroactive β phase nucleation of the *in situ* Fe_2O_3 NPs is greater than the *in situ* Co_3O_4 NPs. Strong interaction between the positive CH_2 charge density of polymer chains and negatively charged surfaces of NPs which leads to long TTTT conformation on the surfaces of the NPs.

Giant dielectric constant of the samples is found to be 6.962×10^3 for 5.1 volume% *in situ* Fe_2O_3 NPs and 6.17×10^4 for 9.5 volume% *in situ* Co_3O_4 NPs at 20 Hz. Brick like shaped Fe_2O_3 NPs leads to lower percolation threshold value or maximum interfacial polarization in PVDF matrix at lower doping (about 5.1 volume%) than the spherically shaped Co_3O_4 NPs.

Thus, the well improved electroactive and colossal dielectric thin films may impact on the development of sensors, actuators and energy storage devices (like super capacitors, solid electrolyte batteries, self-charging power cells etc.).

Acknowledgement

We are grateful to University Grants Commission (UGC), India (F. 17-76/2008 (SA-1)) for the financial assistance.

References

1 T. T. Wang, J. M. Herbert and A. M. Glass, The Applications of Ferroelectric Polymers. *Chapman and Hall:* New York, 1988.

2 H. S. Nalwa, Ferroelectric Polymers: Chemistry, Physics, and Applications. Marcel Dekker: New York, 1995.

3 A. J. Lovinger, Macromolecules, 1981, **14(2)**, 322–325.

4 X. Zhou, B. Chu, B. Neese, M. Lin and Q. M. Zhang, *IEEE Trans. Dielectr. Electr. Insul.* 2007, **14(5)**, 1133-1138.

5 Y. Lu, J. Claude, B. Neese, Q. M. Zhang and Q. Wang, *J. Am. Chem. Soc*. 2006, **128(25),** 8120-8121.

6 N. Karawasa, and W. A. Goddard III, *Macromolecules.*1992, **25 (26)**, 7268–7281.

7 A. B. Silva, M. Arjmand, U. Sundararaj and R. E. S. Bretas, *Polymer*, 2014, **55,** 226-234.

8 V. Tomer, E. Manias and C. A. Randall, *J. Appl. Phys.*, 2011, **110**, 044107-10.

9 P. Thakur, A. Kool, B. Bagchi, S. Das and P. Nandy, *Appl. Clay. Sci,*. 2014, **99**, 149-159.

10 D. Shah, P. Maiti, E. Gunn, D. Schmidt, D. D. Jiang and C. A. Batt, *Adv. Mater.*, 2004, **16(14),**1173–77.

11T. U. Patro, M. V. Mhalgi, D. V. Khakhar and A. Misra, *Polymer* ,2008, **49(16)**, 3486-3499.

12 L. Priya and J. P. Jog, *J. Appl. Polym. Sci.*, 2003, **89(8)**, 2036-2040.

13 P. Mishra and P. Kumar, *Compos. Sci. Technol.*, 2013, **88**, 26-32.

14 T. Zhou, J. W. Zha, R. Y. Cui, B. H. Fan, J. K. Yuan and Z. M. Dang, *ACS. Appl. Mater. Interf.*, 2011, **3(7)**, 2184-2188.

15 Y. Konishi and M. Cakmak., *Polymer*, 2006, **47(15)**, 5371-5391.

16 O. Korostynska, K. Arshak, D. Morris, A. Arshak and E. Jafer, *Mat. Sci. Eng. B*, 2007, **141(3)**,115–20.

17 S. L. Jiang, U. Yu, J. J. Xie, L. P. Wang, Y. K. Zeng and M. Fu, *J. Appl. Polym. Sci.*, 2010, **116(2)**, 838-842.

18 A. Lund, C. Gustafsson, H. Bertilsson and W. Rychwalski, *Compos. Sci. Technol.*, 2011, **71**, 222-229.

19 L. L. Sun, B. Li, Z. G. Zhang and W. H. Zhong, *Eur. Polym. J.*, 2010, **46(11),** 2112-2119.

20 L. L. Sun, B. Li, Y. Zhao, G. Mitchell and W. H. Zhong, Nanotechnology, 2010, 21(30), 305702-10.

21 P. Costa, J. Silva, V. Sencadas, C. M. Costa, F. W. J. van Hattum and J. G. Rocha, *Carbon*, 2009, **47(11)**, 2590–9.

22 Y. J. Li, M. Xu, J. Q. Feng and Z. M. Dang, *Appl. Phys. Lett.* 2006, **89(7)**, 072902–5.

23 J. Wang, J. Wu, W. Xu, Q. Zhang and Q. Fu, *Compos. Sci. Technol*., 2014, **91**, 1-7.

24 H. P. Xu and Z. M. Dang, *Chem. Phys. Lett.*, 2007,**438(4–6),** 196–202.

25 K. S. Deepa, M. S. Gopika and J. James, *Compos. Sci. Technol*. 2013, **78**,18-23.

26 D. Mandal, K. Henkel and D. Schmeißer, *Materials Letters*, 2012, **73**, 123-126.

27 D. Mandal, K. J. Kim and J.S. Lee, Langmuir, 2012, **28(28)**, 10310-10317.

28 P. Martins, C. M. Costa, M. Benelmekki, G. Botelho and S. L. Mendez, *CrystEngComm.*, 2012, **14(8)**, 2807-2811.

29 V. Sencadas, P. Martins, A. Pitães, M. Benelmekki, J. L. G. Ribelles and S. Lanceros-Mendez, *Langmuir*, 2011, **27(11),** 7241-7249.

30 R. Song, G. Xia, X. Xing, L. He, Q. Zhao and Z. Mad, *J. Colloid Interface Sci.*, 2013, **401**, 50-57.

31 W. Wu, X. Huang, S. Li, P. Jiang and T. Toshikatsu, *J. Phys. Chem. C*, 2012, **116(47)**, 24887-24895.

32 Y. Zhang, Y. Wang, Y. Deng, M. Li and J. Bai, *ACS Appl. Mater. Interfaces*, 2012, **4(1)**, 65-68.

33 M. D. Rozana, A. N. Arshad, M. H. Wahid, Z. Habibah, L. N. Ismail, M. N. Sarip and M. Rusop, *Engineering and Industrial Applications*, 2012, *DOI: 10.1109/ISBEIA.2012.6422866*, 18-22.

34 A. S. Bhatt and D. K. Bhat, *Mater. Sci. Eng. B*, 2012, **177(2)**, 127-131.

35 Z. Li, X. Zhang and G. Li, *Phys. Chem. Chem. Phys.*, 2014, **16(12)**, 5475-5479.

36 P. Martins, A. C. Lopes and S. Lanceros-Mendez, *Prog. Polym. Sci.* 2013, **39(4)**, 683-706.

37 P. Nallasamy and S. Mohan, *Ind. J. Pure. Appl. Phys.*, 2005, **43(10)**, 821-827.

38 P. Martins, C. M. Costa, J. C. C. Ferreira and S. Lanceros-Mendez, *J. Phys. Chem. B*, 2012, **116(2)**, 794-801.

39 Y. Li, X. Huang, Z. Hu, P. Jiang, S. Li and T. Tanaka, *ACS Appl. Mater. Interfaces*, 2011, **3(11)**, 4396-4403.

40 T. W. Dakin, *IEEE Electr. Insul. M.*, 2006, **22 (5)**, 11-28.

41 A. Moliton, *Springer*: New York, 2007, Chapter3.

42 C. C. Wang, J. F. Song, H. M. Bao, Q. D. Shen and C. Z. Yang, *Adv. Funct. Mater.*, 2008 **18(8)**, 1299-1306.

43 P. Lunkenheimer, V. Bobnar, A. V. Pronin, A. I. Ritus, A. A. Volkov and A. Loidl, *Phys. Rev. B*, 2002, **66**, 052105-4.

Figure captions:

Figure 1: XRD of pure PVDF and the NPs loaded thin films; (a) Fe_2O_3 NPs loaded PVDF thin films and (b) Co_3O_4 NPs loaded PVDF thin films.

Figure 2: (a) FTIR spectra of pure PVDF and Fe_2O_3 NPs loaded PVDF thin films (PFe 0.01, PFe 0.05, PFe 0.10, PFe 0.15 and PFe 0.20) and (b) Evaluation of β-phase content with increasing Fe_2O_3 NPs content form IR spectra. Error bars represent the standard deviation of the experiment conducted in triplicate and were assessed by one way ANOVA using graph pad Instat version 5.0 software.

Figure 3: (a) FTIR spectra of pure PVDF and Co_3O_4 NPs loaded PVDF thin films (PCo 0.01, PCo 0.05, PCo 0.10, PCo 0.15 and PCo 0.20) and (b) Evaluation of β-phase content with increasing Co_3O_4 NPs content form IR spectra. Error bars represent the standard deviation of the experiment conducted in triplicate and were assessed by one way ANOVA using graph pad Instat version 5.0 software.

Figure 4: (a) DSC thermographs of pure PVDF and Fe_2O_3 NPs loaded PVDF thin films films (PFe 0.01, PFe 0.05, PFe 0.10, PFe 0.15 and PFe 0.20) and (b) DSC thermographs of pure PVDF and Co_3O_4 NPs loaded PVDF thin films (PCo 0.01, PCo 0.05, PCo 0.10, PCo 0.15 and PCo 0.20)

Figure 5: Evaluation of enthalpy of fusion (a, c) and degree of crystallinity (b, d) of pure PVDF and Fe_2O_3/Co_3O_4 NPs loaded PVDF thin films with increasing NPs content from DSC thermographs. Error bars represent the standard deviation of the experiment conducted in triplicate and were assessed by one way ANOVA using graph pad Instat version 5.0 software.

Figure 6: FESEM images of pure PVDF and the Fe_2O_3 NPs loaded PVDF thin films (PFe 0.01, PFe 0.05, PFe 0.10, PFe 0.15 and PFe 0.20).

Figure 7: FESEM images of pure PVDF and and Co_3O_4 NPs loaded PVDF thin films (PCo 0.01, PCo 0.05, PCo 0.10, PCo 0.15 and PCo 0.20).

Figure 8: Zeta potential distribution of (a) Fe_2O_3 NPs and (b) Co_3O_4 NPs.

Figure 9: Schematic diagram of proposed β phase transformation mechanism.

Figure 10: NPs content dependence of dielectric constants and tangent losses at 100 Hz; (a) the Fe_2O_3 NPs loaded PVDF thin films (PFe 0.01, PFe 0.05, PFe 0.10, PFe 0.15 and PFe 0.20) and (b) Co_3O_4 NPs loaded PVDF thin films (PCo 0.01, PCo 0.05, PCo 0.10, PCo 0.15 and PCo 0.20). Error bars represent the standard deviation of the experiment conducted in triplicate and were assessed by one way ANOVA using graph pad Instat version 5.0 software.

Figure 11: NPs content dependence of ac conductivities at 100 Hz, 10 KHz and 1 MHz; (a) the Fe_2O_3 NPs loaded PVDF thin films (PFe 0.01, PFe 0.05, PFe 0.10, PFe 0.15 and PFe 0.20) and (b) Co_3O_4 NPs loaded PVDF thin films (PCo 0.01, PCo 0.05, PCo 0.10, PCo 0.15 and PCo 0.20). Error bars represent the standard deviation of the experiment conducted in triplicate and were assessed by one way ANOVA using graph pad Instat version 5.0 software.

Figure 12: Frequency dependence of dielectric properties of pure PVDF and Fe_2O_3/ Co_3O_4 NPs loaded PVDF thin films; (a, d) dielectric constants, (b, e) tangent losses and (c, f) ac conductivities.

Table 1: Different amount of *in situ* synthesized Fe_2O_3 or Co_3O_4 NPs in the polymer matrix.